Atmospheric
Measurement
Techniques
Discussions

1   **Reactive mercury flux measurements using cation exchange membranes**

2   Matthieu B. Miller[1*], Mae S. Gustin[2], Grant C. Edwards[1,3]

3   [1]Faculty of Science and Engineering, Department of Environmental Science, Macquarie University, Sydney, NSW,
4   2113, Australia

5   [2]Department of Natural Resources and Environmental Science, University of Nevada, Reno NV, 89557, United
6   States

7   [3]Deceased 10 September 2018.

8   *Correspondence to*: Mae Sexauer Gustin mgustin@cabnr.unr.edu

9   **ABSTRACT**

10   A method was developed to measure gaseous oxidized mercury (GOM) air-surface exchange

11   using 2 replicated dynamic flux chambers (DFCs) in conjunction with cation exchange

12   membrane (CEM) filters. The experimental design and method was developed and tested in a

13   laboratory setting, using materials collected from industrial scale open pit gold mines in central

14   Nevada, USA. Materials used included waste rock, heap leach ore, and tailings, with substrate

15   concentrations ranging from 0.1 to 40 μg g^{-1} total mercury (THg). CEM filters were used to

16   capture GOM from the DFC sample lines while a Tekran® 2537A analyzer measured GEM

17   concurrently. Previous and ongoing work demonstrated that CEM do not collect GEM and

18   efficiently collects multiple compounds of GOM. Positive GOM emission rates up to 4000 pg m^{-2}

19   ^{2} h^{-1} were measured from tailings materials with high Hg substrate concentrations, and this has

20   significant implication with respect to air-Hg surface exchange. GOM flux was variable for

21   lower Hg concentration substrates, with both emission and deposition observed, and this

22   wasaffected by ambient air GOM concentrations. For substrates that experienced GOM

23   deposition, deposition velocities were in the range 0.01 – 0.07 cm s^{-1}.

24

25

1 Introduction

27 On 16 August 2017, the United Nations Environment Program (UNEP) Minamata Convention

28 came into force with a mission to protect human health and the environment from exposure to

29 the toxic effects of mercury (Hg) and its various compounds (UNEP, 2013). The Convention

30 proposes to fulfill this mission through a strategy of globally coordinated scientific research, and

31 ongoing monitoring of Hg in the environment where possible. The mission poses a significant

32 challenge as there are over 3000 known Hg contaminated sites worldwide due to mining and

33 industrial activity, not including legacy and small scale operations involving Hg (Kocman et al.,

34 2013; Krabbenhoft and Sunderland, 2013). Past emissions were dominantly from natural sources,

35 but are now largely from anthropogenic activities and have led to large reservoirs of Hg in all

36 environmental compartments (Pacyna et al., 2016; Pirrone et al., 2010; Streets et al., 2017). Even

37 in the absence of new anthropogenic emissions, cycling of Hg between different spheres will

38 continue at large scales and in possibly unexpected directions, driven by processes and

39 mechanisms that are not fully understood, and susceptible to increasing human and climate

40 perturbations (Obrist et al., 2018).

41 The atmosphere, a global common, is the dominant conduit for transport, transformation,

42 emission, deposition, and re-emission of Hg and Hg compounds amongst Earth's ecosystems.

43 Mercury in the atmosphere is classified on the basis of three physiochemical forms: gaseous

44 elemental mercury (GEM), gaseous oxidized mercury (GOM), and particulate bound mercury

45 (PBM), with PBM and GOM defined together as reactive mercury (RM = GOM + PBM)(Gustin

46 et al., 2015). Atmospheric concentrations of GEM can be measured with well calibrated

Atmospheric
Measurement
Techniques
Discussions

47   analytical instruments, whereas the quantification of GOM and PBM has depended on

48   operationally defined methods with demonstrably large uncertainty (Cheng and Zhang, 2017;

49   Gustin et al., 2015; Gustin et al., 2013; Jaffe et al., 2014; Zhang et al., 2017).

50   Scientific understanding of the biogeochemical cycling of Hg is currently inadequate due to the

51   large uncertainties in measurements, and general difficulty of research on atmospheric Hg

52   chemistry (Jaffe et al., 2014). Atmospheric GEM is relatively inert, has a low deposition rate,

53   and hence a relatively long atmospheric lifetime ranging from minutes to 1 year (Krabbenhoft

54   and Sunderland, 2013; Zhang et al., 2009; Gustin et al., 2013). Observations of rapid depletion

55   of GEM from the atmosphere suggests that deposition and re-emission on short time scales is an

56   important process driving movement (Howard and Edwards, 2018; Lu et al., 2001; Schroeder et

57   al., 1998). In contrast to GEM, GOM compounds have higher dry deposition velocities (Zhang et

58   al., 2009). Knowledge of concentrations, chemistry, and processes forming atmospheric GOM is

59   critical for understanding how Hg moves and impacts ecosystems globally. Recent research on

60   GOM has demonstrated that compounds in air vary both spatially and temporally to a

61   considerable extent, pointing to the need for extensive measurements of concentrations and

62   identifying the specific compounds (Gustin et al., 2016; Huang and Gustin, 2015b; Huang et al.,

63   2014; Huang et al., 2017).

64   Fluxes of total gaseous mercury (TGM) and GEM have been successfully measured in many

65   environments, providing insights into air-surface exchange that is critical for understanding

66   biogeochemical cycling of GEM (Yannick et al., 2016; Zhu et al., 2016). In contrast, there are

67   few direct measurements of GOM air-surface exchange (Zhang et al., 2009). GOM fluxes

68   reported in the literature are largely based on measurements made with the KCl denuder as the

69   GOM collection method, as well as a passive Hg dry deposition sampler (Brooks et al., 2008;

70   Castro et al., 2012; Engle et al., 2005; Lindberg et al., 2002; Lindberg and Stratton, 1998; Lyman

71   et al., 2009; Lyman et al., 2007; Malcolm and Keeler, 2002; Poissant et al., 2004; Rea et al.,

72   2000; Rothenberg et al., 2010; Sather et al., 2013; Skov et al., 2006; Zhang et al., 2005; Huang et

73   al., 2015b). The few direct GOM-specific air-surface exchange measurements using KCl

74   denuder-based approaches have been undertaken with mixed results (Brooks et al., 2008; Skov et

75   al., 2006). Moreover, recent evaluation of KCl denuder approaches show these methods tend to

76   underestimate GOM and are subject to interferences due to ozone and water vapor (Huang and

77   Gustin, 2015a; Lyman et al., 2010; McClure et al., 2014). Understanding GOM air-surface

78   exchange processes would facilitate the Hg scientific community's ability to move forward in

79   understanding the biogeochemical cycling of atmospheric Hg.

80   In this study, we developed and applied a novel experimental approach for direct measurement

81   of GOM fluxes using cation exchange membrane (CEM) filters. CEM filters have been

82   successfully deployed to measure GOM in ambient air in previous studies (Gustin et al., 2016;

83   Huang et al., 2017; Huang et al., 2013; Marusczak et al., 2017; Pierce and Gustin, 2017), and

84   their use here was modified to allow for the determination of GOM air-surface exchange. A

85   recent study (Miller et al., 2018) and ongoing work (unpublished data) have demonstrated that

86   GEM is not collected by the CEM and it efficiently collects a variety of GOM compounds. Here

87   is described a series of experiments that were conducted to optimize the CEM/GOM flux

88   methodology, and then, the resulting method was subsequently applied to determine fluxes over

89   both background waste rock material and Hg enriched mining materials. Our research

90   hypothesis was the system developed would provide a means of determining if GOM is

Atmospheric
Measurement
Techniques
Open Access
Discussions

91   deposited or emitted from substrates, and this system would allow us to develop an

92   understanding of GOM air-surface exchange.

93   **Methods**

94   **2.1 Materials**

95   Substrate materials used for measuring Hg flux were acquired from industrial scale, open pit

96   gold mines in central Nevada, and include waste rock, heap leach ore, and tailings. Materials

97   were obtained from 4 ongoing mining operations: Twin Creeks (TC) and Lone Tree (LT)

98   operated by Newmont Mining Corporation, and Cortez Pipeline (CP) and Gold Strike (GS)

99   operated by Barrick Gold Corporation (Fig. 1; Table 1). There were 3 types of materials: waste

100 rock called cap (C), heap leach material (L), and tailings (T or tails). (Waste rock is non-

101 mineralized low Hg overburden consisting of alluvium or hard rock that covered the ore body

102 prior to mining. For this study, materials were sampled from the waste rock piles specifically set

103 aside for future capping and site reclamation, and as such is referred to as cap material. Heap

104 leach is low-grade ore blasted from the mine wall and "heaped" on an impoundment for

105 irrigation with dilute cyanide leach solution for gold extraction. Tailings are the waste remnant

106 of high-grade ore that has been pulverized by mechanical ball milling and undergone

107 thermal/chemical treatment to extract gold. All mining substrate materials were collected in

108 September 2010, for measurements of GEM flux under controlled conditions (Miller and Gustin,

109 2013).

110   Each material was divided into replicate trays (50 x 50 x 7 cm^3 plywood lined with 3mil

111 polyvinyl sheet) and stored inside a greenhouse bay at the University of Nevada Reno

112   Agricultural Experiment Complex. At the onset of the GOM flux experiments described in this

113   paper, substrates were undisturbed for ~3 years, and were completely dry and well

114   compacted/consolidated from previous watering experiments. A circular chamber footprint

115   impression previously existed from prior experiments provided an excellent existing contact for

116   the chamber base. Comparing GEM flux measurements made in this study with the previous

117   measurements, an overall trend of decreasing GEM flux over time was observed. This fits a

118   hypothesis suggested by Eckley et al. (2011b) of a long term reduction in GEM evasion from a

119   mine substrate as time from disturbance increases.

120   **2.2 Methodology**

121   GOM flux was measured by modifying our existing GEM flux method consisting of a dynamic

122   flux chamber (DFC) and an ambient air Hg analyzer (Tekran® 2537A) after the methods of

123   Eckley et al. (2010; 2011a) and Miller et al. (2011).

124   Briefly, the GEM flux system used a 2537A in conjunction with a cylindrical DFC (footprint

125   0.036 m^2) made of molded Teflon film (0.19 mm thick) over a rigid Teflon frame (1.5 mm

126   thickness), with a total internal volume of 2.0 Liters (Fig. 2). Air enters the chamber through 24

127   inlet holes (1 cm diameter) spaced 2.5 cm apart around the perimeter and 2.0 cm above the

128   bottom edge. The sample outlet is 0.625 cm diameter PTFE tubing at the top-center of the

129   chamber, and sample inlet air is measured through equivalent tubing at the height of the chamber

130   inlet holes. A Tekran® Automated Dual Switching (TADS) unit was used to cycle the sample

131   flow (1.0 Lpm) between the chamber inlet and outlet lines in sequential 10 min intervals (two 5

132   min samples on each line). GEM in each 5 min sample volume was quantified automatically by

133   the 2537A analyzer using pre-concentration on gold traps followed by thermal desorption (500

Atmospheric
Measurement
Techniques
Discussions
Open Access

134   °C) and cold vapor atomic fluorescence spectrometry (CVAFS). The difference in Hg

135   concentration between the outlet and inlet air (C_o – C_i) referred to as ΔC, and was used to

136   calculate flux by Eq. 1:

137                          $$F = Q * (C_o - C_i)/A \quad (1)$$

138   where F is the net Hg flux (ng m^{-2} h^{-1}), Q is the flow rate through the chamber (m^3 h^{-1}), C_o is the

139   mean concentration of two consecutive 5 min outlet air samples (ng m^{-3}), C_i is the mean

140   concentration of inlet air in the samples before and after C_o, and A is the area of the substrate

141   under the chamber (m^2). The sign of ΔC indicates the direction of flux with positive being

142   emission and negative being deposition.

143   The two modified systems included fitting the DFC inlet and outlet sample lines with 2-stage

144   disc filter assemblies (Savillex$^©$ 47 mm PFA Teflon Filter Holder) holding two inline

145   polysulfone cation exchange membranes (CEM 0.8 µm, Mustang$^®$ S, Pall Corporation) (Fig. 2).

146   CEMs preferentially capture GOM compounds while allowing GEM to pass freely (Miller et al.

147   2018; unpublished data). The first upstream CEM served as the primary collection filter, while

148   the second downstream CEM captured any Hg escaping from or missed by the first filter

149   (referred to as breakthrough). With CEM filters deployed at the front of the sample lines, in

150   conjunction with the 0.2 µm particulate filter at the rear sample inlet of the Tekran$^®$, GOM was

151   scrubbed from the sample flow and all Hg measured downstream on the 2537A is in GEM form.

152   An additional set of CEM filters was deployed simultaneously, using sample pumps and mass

153   flow controllers set to match the 2537A sample flow rate (1.0 Lpm, Fig. 2) at a height of 2 m

154   above the flux system. This was done to measure background ambient GOM concentrations in

155   the greenhouse.

156   With both the Tekran® and external pump controlling CEM sample lines at 1 Lpm, total flow

157   through the DFC was 2.0 Lpm that provides a chamber turn over time (TOT) of 1 minute. At this

158   flow rate, flow velocity through the chamber is laminar with no turbulent eddy formation, as

159   determined through computational fluid dynamic (CFD) modelling of the chamber geometry

160   performed by Eckley et al. (2010). Thus the chamber design of Eckley et al. (2010) is optimal in

161   terms of not disturbing the substrate being studied. With low velocity, non-turbulent flow,

162   particle entrainment from the substrate surfaces is not expected, especially for particle sizes

163   greater than the CEM filter pore size of 0.8 μm.

164   **2.3 Analyses**

165   After flux measurements, CEM filters were collected into sterile 50 mL polypropylene centrifuge

166   tubes, and frozen at -20 °C until analyses (within 14 days of collection). Filters were analyzed for

167   total Hg by aqueous digestion and cold vapor atomic fluorescence spectrometry (CVAFS, EPA

168   Method 1631, Rev. E) using a Tekran 2600 system, with total Hg operationally equivalent to

169   total GOM. The blank Hg mass that can be expected on an unused CEM filter (median = 68 pg, n

170   = 56) was determined from clean filters collected with every set of measurements, and the

171   median blank value was subtracted from all sample values. Breakthrough is defined as the

172   amount of Hg on the secondary filter as a percent of the total Hg collected on both filters (after

173   blank correction), and overall median breakthrough was low (4.2%, n = 222).

Atmospheric
Measurement
Techniques
Discussions

174 The GOM concentration in the inlet/outlet sample air was calculated by combining the blank-

175 corrected primary and secondary filters into a total Hg mass per sample line and dividing by the

176 respective sample air volume. The difference in GOM concentration between the inlet and outlet

177 lines provided a ΔC_{GOM}, with this multiplied by sample flow providing the GOM emission rate

178 (pg h^{-1}). Reactive Hg flux (pg m^{-2} h^{-1}) was calculated with Eq. 1 using ΔC_{GOM} values, the flow

179 rate (1.0 ± 0.005 Lpm) and the chamber footprint (0.036 m^2).

180 The GOM flux detection limit was determined by the minimum statistically resolvable difference

181 between C_o and C_i, i.e. the smallest meaningful ΔC_{GOM} that could be measured (Fig. 3). The C_o

182 and C_i concentrations were based on two measurements: total Hg on the CEM filters as

183 determined by analysis on the Tekran® 2600 system, and total sample volume as determined by

184 the mass flow-controlled sample rate and time. The MFC precision was ± 0.5% (± 0.005 Lpm at

185 1.0 Lpm) and the detection limit of the 2600 was 1 ppt, or ~ 53 pg per reagent blank in a clean 50

186 mL collection tube. The median mass of Hg on the blank CEM filters was 68 pg and was used as

187 the practical detection limit for the method. As the distribution of CEM blank values was non-

188 normal and skewed heavily to the right (Fig. 3a), the 95% confidence interval around the median

189 (58 – 73 pg) was used to define a minimum detectable GOM concentration (Fig. 3b). For

190 example, in a 24 h sample, the minimum detectable GOM concentration would be ~ 3.5 pg m^{-3} to

191 exceed the upper 95% confidence limit of 73 pg. In a 24 h sample the minimum resolvable

192 ΔC_{GOM} would be 13.5 pg m^{-3} (sum of upper + lower confidence intervals, + 3 pg m^{-3} to account

193 for flow precision, converted to 24 h sample volume concentration). This was taken as the upper

194 minimum ΔC_{GOM} value.

195   Chamber blanks were determined for each Teflon DFC (referred to as Chamber A and Chamber

196   B) by measuring flux over a clean Teflon sheet. Chamber blank emission rates were measured

197   immediately following chamber cleanings (24 h acid wash, 10% HNO_3), and then between

198   substrate types (i.e. cap, leach, tailings). For the summer measurement period, the median

199   chamber blank ΔC_{GOM} for both Chambers A and B (A = 13 pg m^{-3}, B = 14 pg m^{-3}, n = 12) was at

200   the detection limit, so chamber blanks were not subtracted from material fluxes. This was due to

201   high ambient GOM concentrations in the greenhouse. For the following winter measurement

202   period, the median chamber blank ΔC_{GOM} for both chambers was significantly negative (A = -60

203   pg m^{-3}, B= -60 pg m^{-3}, n = 6), and the median chamber blank was -215 pg m^{-2} h^{-1}, indicating that

204   the chamber and the blank Teflon sheet were acting as depositional surfaces for GOM. For these

205   measurements, the chamber blanks were subtracted. For materials that demonstrated net GOM

206   deposition, the deposition velocity (V_d cm s^{-1}) was calculated using Eq. 2:

207    $$V_d \ = \ \text{flux} \ (ng \ m^{-2} \ h^{-1}) \ / \ \text{air concentration} \ (ng \ m^{-3}) \ * \ (100/3600) (2)$$

208   All fluxes were measured in the University of Nevada-Reno Agricultural Experiment Station

209   greenhouse. Meteorological parameters were measured synchronously with flux and recorded in

210   5 min averages, including temperature and relative humidity (HMP45C, Campbell Scientific®),

211   substrate temperature (C107, Campbell Scientific®), and solar radiation (LI-200X, LiCor®).

212   Rudimentary climate control was provided by ventilation fans pulling outside air across the

213   greenhouse bay from intakes on the opposite side. Fluxes were measured on the "upwind" side

214   of the bay in a variety of orientations (see below).

215   Data was processed in Microsoft Excel (version 16.22) and RStudio® (version 3.2.2).

Atmospheric
Measurement
Techniques
Discussions

2.4 Development of the method

217   Two Tekran® 2537A analyzers with associated GOM filter systems were used to simultaneously

218   measure flux from two replicate trays (one for each A and B system) of each sample material.

219   The duplicated systems allowed a total of four GOM flux measurements to be collected each

220   time a material was tested, two from the Tekran® sample lines and two from the external pump

221   lines. The intention of the duplicate systems was to evaluate consistency and repeatability of the

222   measurements. However, during the initial method testing it became apparent that the position of

223   the trays and the inlet sample lines was an important variable. For example, strong GOM

224   emission from an "upwind" tray could substantially increase the inlet GOM concentration of the

225   "downwind" tray, resulting in a negative ΔC_{GOM} and apparent deposition. Such contradictory

226   results compelled us to test a variety of orientations for the two systems. The best results were

227   achieved in the final design by placing both trays all the way against the intake wall of the

228   greenhouse bay, and separating them laterally by 1.5 m, with all equipment located downwind.

229   This configuration provided the most uniform inlet air concentrations for both systems.

2.5 Limitations of method

231   The use of filter membranes in conjunction with a DFC to measure GOM flux has several

232   limitations. Given the low concentrations of GOM, a relatively long sampling time of at least 24

233   h is required to capture a sufficient mass for quantification on low Hg containing substrates.

234   Despite the limitations, this method moves us a step further for understanding GOM flux. The

235   low temporal resolution limits analysis of the factors controlling GOM flux, since there will be

236   changes on a diel cycle similar to observations of GEM flux (c.f. Gustin et al., 2013). In

237   addition, flow rate and surface area could be increased, but in order to change this method a

238   number of proof of concept tests would have to be done.

239   A necessary condition of the DFC method is the placement of flux chambers directly on a

240   material, resulting in artificial modification of surface conditions and a presumptive influence on

241   the magnitude of flux. In our study, this limitation is immaterial, as the entire experimental setup

242   constitutes an artificial environment, and we are more interested in 1) our ability to

243   experimentally detect measurable GOM flux, and 2) the qualitative direction of flux versus

244   absolute quantification. As the method develops, it will become necessary to more thoroughly

245   evaluate the effects of the DFC on GOM flux.

246   Lastly, CEM were analyzed within two weeks of collection. Pierce et al. (2017) demonstrated

247   that little $HgCl_2$ was lost from the membranes over this time period. This needs to be tested for

248   other GOM compounds thought to be present in the atmosphere (Huang et al., 2013; Gustin et

249   al., 2016).

250   **3   Results**

251   **3.1 GOM flux measurement repeatability**

252   The first test of the optimized configuration was a set of replicate measurements made on a

253   single material, to assess method repeatability. The material used for this test was a heap leach

254   ore of intermediate total Hg concentration (TCL, 13.2 ± 2.0 µg g^{-1}). Filters were deployed in

255   three consecutive sample sets of approximately 72 h each, for a total of 12 replicate filter flux

256   measurements (i.e. two GOM flux measurements on two separate replicate trays, three times).

257   The mean GEM flux from all samples was 167 ± 57 ng m^{-2} h^{-1} (n = 6). The duplicate

258   measurements of background greenhouse GOM showed a mean concentration of 13 ± 7 pg m^{-3}

259   (n = 12). The ΔC_{GOM} was well above detection for all measurements (median 97 pg m^{-3}, n = 12),

260   and the mean GOM flux over all 12 samples was 370 ± 80 pg m^{-2} h^{-1} (n = 12) and ranged from

261   240 to 490 pg m^{-2} h^{-1} (Fig. 4).

262   The mean relative percent difference (RPD) of GOM flux measured between Pump and Tekran

263   sample lines on the same tray was $6.5 \pm 3.9\%$, and mean RPD between trays was 21.4%. These

264   replicate measurements of a single material consistently showed the same direction and

265   magnitude of GOM flux with good agreement.

266   3.2 **GOM flux measurement replication over expanded range of materials: Summer**

267   Following the triplicate measurement of TCL (May), follow up testing was conducted on a series

268   of three additional materials (July – August): a low to intermediate Hg cap material and heap

269   leach ore (TCC 0.2 µg g^{-1}, LTL 0.6 µg g^{-1}), and a high Hg tailings (TCT 36 µg g^{-1}).

270   Measurement time was reduced to 48 h for this series of materials, as the previous deployments

271   had total GOM loading well above detection. However, several of the LTL and TCC flux

272   measurements resulted in insignificant ΔC_{GOM} values (Fig. 5). In these cases, GOM flux could

273   not be discriminated, and these values were excluded from subsequent analysis.

274   A comparison of GOM flux measured by the replicate sample lines on each system (Tekran$^{®}$

275   sample flow and external pump sample flow) show a relationship of 1:1 (Fig. 6) that indicates

276   that CEM filters on two independent flow channels were capturing equivalent amounts of GOM.

277   This equivalency was true for both of the replicate systems (System A and B) that were each

278   simultaneously measuring flux from replicate trays of the same material. The high level of

Atmospheric
Measurement
Techniques
Open Access
Discussions

279   replication displayed by the system, both in general and in detail, for multiple substrate types,

280   increases confidence that these measurements represent a real net surface exchange of GOM.

281   Positive GOM fluxes were associated with the higher substrate concentration materials (TCL,

282   TCT). The low Hg TCC experienced net GOM deposition, with a mean V_d of 0.03 ± 0.01 cm s^{-1}

283   (n = 6). The 3x higher Hg concentration LTL showed either no net flux or slightly positive GOM

284   emission (64 ± 10 pg m^{-2} h^{-1}, n = 3). The very high substrate Hg concentration TCT$^-$ materials

285   showed uniformly high GOM emission (4060 ± 1000 pg m^{-2} h^{-1}, n = 7).

286   The mean ambient GOM in the greenhouse during this period was 130 ± 55 pg m^{-3} (n = 24);

287   however, there was a distinct trend of increasing ambient GOM over the course of

288   measurements. During the TCC measurements, ambient GOM concentration in the greenhouse

289   was 70 ± 20 pg m^{-3} (n = 8). This increased to 150 ± 20 pg m^{-3} (n = 8) during the LTL

290   measurements, and up to 180 ± 40 pg m^{-3} (n = 8) during the TCT measurement.

291   **3.3 GOM flux measurement over complete range of materials: Winter**

292   A full set of 24 h GOM flux measurements including all the available mining materials was

293   made in the following winter period (January – March, 2016). Ambient GOM concentration in

294   greenhouse air was 50 pg m^{-3} (n = 16), much lower than in the summer months. Mean RH and

295   solar radiation were similar between the summer and winter periods, due to the attenuating effect

296   of the greenhouse. However, mean air and substrate temperatures were significantly lower in the

297   winter (Table 1).

298   All measured fluxes were above the ΔC_{GOM} detection limit (Fig. 7a). The relationship between

299   GOM flux measured on the A and B systems was slightly less than 1:1 (B = 0.87*A) and not as

Atmospheric
Measurement
Techniques
Discussions

300 strong ($r^2 = 0.74$) as during the summer measurements. Without chamber blank correction, GOM

301 fluxes were uniformly negative for all materials except the very high Hg TCT (Fig. 7b, orange

302 shades). However, with the chamber blank correction applied, GOM flux from the cap materials

303 became ambiguous (i.e. both deposition and emission observed) and positive for all leach and

304 tailings materials except the LTT (Fig. 7c, green shades).

305 Three replicated materials had consistent fluxes, with or without blank correction: GS cap (GOM

306 deposition, $V_d = 0.02 - 0.04$ cm s^{-1}, corrected), LTT (GOM deposition, $V_d = 0.01 - 0.05$ cm s^{-1},

307 corrected), and TCT (strong GOM emission). The GS mine exploits a predominantly

308 carbonaceous ore deposit, and much of the mine and surrounding areas are subject to carbon

309 loading from aerial dust deposition. The carbon in the GS waste rock and ore likely facilitate

310 deposition of Hg and GOM (c.f. Miller et al, 2013 ; Eckley et al., 2011), . The LTT material is

311 from a non-active tailings impoundment that was partially revegetated at the time of collection,

312 versus the entirely barren surface typical of active tailings. Although the LTT Hg concentration

313 was high (11 µg g^{-1}), the surface was old, and it is possible this material behaved more as a

314 background substrate. The TCT material was collected from an actively filling tailings

315 impoundment that collected process waste from a variety of ore types, from multiple mine sites,

316 and had the highest Hg concentration of the materials used in this study, which likely explains its

317 tendency to by a strong emitter of both GEM and GOM, a conclusion also made by Eckley et al.

318 (2011a).

319 An interesting point is that background (2 m and inlet GOM concentrations were very similar

320 during the summer measurements (Fig. 8a), but inlet concentrations were 3x higher than

321 background during the winter measurements (Fig. 8b). The lower winter background GOM (50

Atmospheric
Measurement
Techniques
Discussions

322   pg m^{-3}) compared to summer (110 pg m^{-3}) may partially explain this, however the distance

323   between the inlet and background sampling heights was only ~ 1 m, which implies a strong

324   vertical gradient in GOM concentration in the greenhouse air. The explanation for this is less

325   well mixed air in the greenhouse bay during the winter, as the greenhouse circulation was shut

326   down at temperatures approaching 13 °C, setting up stratified conditions. The relatively high

327   inlet level GOM concentrations during the winter also caused the higher deposition observed in

328   the chamber blank measurements during this time.

329   **4   Conclusions**

330   This study presents direct GOM flux measurements using a CEM filter technique and provides

331   an analysis of whether the necessary measurements of small differences in GOM concentration

332   were possible using a DFC method. Measurements of GOM flux were above calculated

333   detection limits in most cases, and both intra- (Tekran vs Pump sample) and inter- (A vs B)

334   system replicate measurements showed very good agreement. After initial trials at 72 h and 48 h,

335   a 24 h sample time was found to be generally sufficient for detecting GOM flux on the mining

336   materials used in this study, some of which were similar to background soils. It would be

337   possible to operate the system at higher flow rates, to decrease sample time and improve the

338   temporal resolution of the flux measurements. However, sample deployment and collection

339   require 20-30 min and to some extent perturbs the system, so ultimately the flux resolution is

340   limited by practical operational constraints. The 24 h measurement at least serves to capture net

341   flux over a full diel cycle without continuous interruptions.

342   We specifically refer to our measurement as GOM. This is because particulate Hg is not *emitted*

343   from a surface in the volatile sense, and particle entrainment was negligible at the low flow

Atmospheric
Measurement
Techniques
Discussions

344   velocities generated in the flux chambers. Thus GOM concentrations measured at the chamber

345   outlet CEM filters are dominated by GOM. If ambient air GOM concentrations were primarily

346   PBM, at a size fraction large enough to be captured by the CEM filters (i.e. > 0.8 μm), it will

347   undeniably be captured at the chamber inlet filters. However, PBM at this size would likely

348   deposit to the substrate surface within the chamber, thus deposition is GOM loading on the C_o

349   filters versus the C_i filters.

350   Here we have demonstrated that GOM can be deposited and emitted from a surface. It is unlikely

351   GOM was produced by oxidation of GEM given short time of air moving through the chamber

352   and the fact that strong oxidants were likely removed as air moved through air handlers into the

353   greenhouse. This is a unique scientific finding. Flux measured from low Hg, non-mineralized

354   cap materials for both GEM and GOM were low positive and negative values oscillating around

355   a net zero flux (Table 1). The observed GEM deposition velocities were typical of non-vegetated

356   surfaces, while GOM deposition occurred at V_d values (0.01 – 0.07 cm s^{-1}) on the low end of the

357   suggested range (Zhang et al., 2009). The higher Hg concentration leach and tailings material

358   (except LT tails) showed net GEM and GOM emission in the summer, while deposition was

359   observed for both for most materials in the winter. The highest GOM emissions were

360   consistently observed for the highest Hg concentration substrate, TCT, in both summer and

361   winter conditions with fluxes higher in the summer during which time the greenhouse was better

362   mixed. The implications of these results are that GOM fluxes may be directly measured and that

363   contaminated areas such as mine tailings impoundments can act as a direct emission source of

364   GOM compounds to the atmosphere.

365

366   **Acknowledgements**

Atmospheric
Measurement
Techniques
Discussions

370

371

References

373   Brooks, S., Arimoto, R., Lindberg, S., and Southworth, G.: Antarctic polar plateau snow surface
374   conversion of deposited oxidized mercury to gaseous elemental mercury with fractional
375   long-teGOM burial, Atmospheric Environment, 42, 2877-2884, 2008.

376   Castro, M. S., Moore, C., Sherwell, J., and Brooks, S. B.: Dry deposition of gaseous oxidized
377   mercury in Western Maryland, Science of the Total Environment, 417-418, 232-40, 2012.

378   Cheng, I., and Zhang, L.: Uncertainty Assessment of Gaseous Oxidized Mercury Measurements
379   Collected by Atmospheric Mercury Network, Environmental Science & Technology, 51,
380   855-862, 2017.

381   Eckley, C. S., Gustin, M., Lin, C. J., Li, X., and Miller, M. B.: The influence of dynamic
382   chamber design and operating parameters on calculated surface-to-air mercury fluxes,
383   Atmospheric Environment, 44, 194-203, 2010.

384   Eckley, C.S., Gustin, M., Marsik, F., and Miller, M.B.: Measurement of surface mercury fluxes
385   at active industrial gold mines in Nevada (USA), Science of the Total Environment, 409,
386   514-522, 2011a.

387   Eckley, C. S., Gustin, M., Miller, M.B., and Marsik, F.: Scaling Non-Point-Source Mercury
388   Emissions from Two Active Industrial Gold Mines: Influential Variables and Annual
389   Emission Estimates, Environmental Science & Technology, 45, 392-399, 2011b.

390   Engle, M. A., Sexauer Gustin M, Lindberg, S. E., Gertler, A.W., and Ariya, P.A. : The influence
391   of ozone on atmospheric emissions of gaseous elemental mercury and reactive gaseous
392   mercury from substrates, Atmospheric Environment, 39, 7506-7517, 2005..

393   Gustin, M. S., Amos, H.M., Huang, J., Miller, M.B., and Heidecorn, K.: Measuring and
394   modeling mercury in the atmosphere: a critical review, Atmos. Chem. Phys. 15: 5697-
395   5713, 2015.

396   Gustin, M. S., Huang, J., Miller, M. B, Peterson C., Jaffe, D. A., Ambrose, J, et al.: Do We
397   Understand What the Mercury Speciation Instruments Are Actually Measuring? Results
398   of RAMIX, Environmental Science & Technology, 47, 7295-7306, 2013.

399 Gustin, M. S., Pierce, A.M., Huang, J., Miller, M.B., Holmes, H.A., and Loria-Salazar, S.M.:
400   Evidence for Different Reactive Hg Sources and Chemical Compounds at Adjacent
401   Valley and High Elevation Locations, Environmental Science & Technology, 50, 12225-
402   12231, 2016.

403 Howard, D., and Edwards, G.C.: Mercury fluxes over an Australian alpine grassland and
404   observation of nocturnal atmospheric mercury depletion events, Atmos. Chem. Phys., 18,
405   129-142, 2018.

406 Huang, J. and Gustin, M.S.: Uncertainties of Gaseous Oxidized Mercury Measurements Using
407   KCl-Coated Denuders, Cation-Exchange Membranes, and Nylon Membranes: Humidity
408   Influences, Environmental Science & Technology, 49, 6102-6108, 2015a.

409 Huang, J. and Gustin, M.S.: Use of Passive Sampling Methods and Models to Understand
410   Sources of Mercury Deposition to High Elevation Sites in the Western United States;
411   Environmental Science & Technology, 49, 432-441, 2015b.

412 Huang, J., Lyman, S.N., Hartman, J.S., and Gustin, M.S.: A review of passive sampling systems
413   for ambient air mercury measurements, Environmental Science: Processes & Impacts 16:
414   374-392, 2014.

415 Huang, J., Miller, M.B., Edgerton, E., and Sexauer Gustin, M. Deciphering potential chemical
416   compounds of gaseous oxidized mercury in Florida, USA, Atmos. Chem. Phys., 17,
417   1689-1698, 2017.

418 Huang, J., Miller, M.B., Weiss-Penzias, P., and Gustin, M.S.: Comparison of Gaseous Oxidized
419   Hg Measured by KCl-Coated Denuders, and Nylon and Cation Exchange Membranes,
420   Environmental Science & Technology, 47, 7307-7316, 2013.

421 Jaffe, D. A., Lyman, S., Amos, H.M., Gustin, M. S., Huang, J., Selin, N.E., et al.: Progress on
422   Understanding Atmospheric Mercury Hampered by Uncertain Measurements.
423   Environmental Science & Technology, 48, 7204-7206, 2014.

424 Kocman, D., Horvat, M., Pirrone, N., and Cinnirella, S.: Contribution of contaminated sites to
425   the global mercury budget. Environmental Research, 125, 160-170, 2013.

426 Krabbenhoft, D.P. and Sunderland E. M.: Global Change and Mercury, Science, 341, 1457,
427   2013.

428 Lindberg, S.E., Brooks, S., Lin, C.J., Scott, K. J., Landis, M.S., Stevens, R.K., et al.: Dynamic
429   Oxidation of Gaseous Mercury in the Arctic Troposphere at Polar Sunrise;
430   Environmental Science & Technology, 36, 1245-1256, 2013.

431 Lindberg, S.E., and Stratton, W.J.: Atmospheric mercury speciation: Concentrations and
432   behavior of reactive gaseous mercury in ambient air, Environmental Science &
433   Technology 32: 49-57.

Atmospheric
Measurement
Techniques
Discussions

434   Lu, J., Schroeder, W., Barrie, L., Steffen, A., Welch, H., Martin, K., et al.: Magnification of
435   atmospheric mercury deposition to polar regions in springtime: the link to tropospheric
436   ozone depletion chemistry, Geophysical Research Letters, 28, 3219-3222, 2001.

437   Lyman, S.N, Gustin, M. S., Prestbo, E. M., Kilner, P. I., Edgerton, E., Hartsell, B.:Testing and
438   Application of Surrogate Surfaces for Understanding Potential Gaseous Oxidized
439   Mercury Dry Deposition, Environmental Science & Technology, 43, 6235-6241, 2009.

440   Lyman, S.N., Gustin, M. S., Prestbo, E.M., and Marsik, F.J.: Estimation of Dry Deposition of
441   Atmospheric Mercury in Nevada by Direct and Indirect Methods, Environmental Science
442   & Technology, 41, 1970-1976, 2007.

443   Lyman, S.N., Jaffe, D. A., and Gustin, M.S.: Release of mercury halides from KCl denuders in
444   the presence of ozone, Atmospheric Chemistry and Physics, 10, 8197-8204, 2010.

445   Malcolm, E.G., and Keeler, G.J.: Measurements of mercury in dew: atmospheric removal of
446   mercury species to a wetted surface, Environmental Science & Technology, 36, 2815-
447   2821, 2002.

448   Maruszczak N, Sonke JE, Fu X, Jiskra M. Tropospheric GOM at the Pic du Midi Observatory—
449   Correcting Bias in Denuder Based Observations. Environmental Science & Technology
450   2017; 51: 863-869.

451   McClure, C. D., Jaffe, D.A., and Edgerton, E.S.: Evaluation of the KCl Denuder Method for
452   Gaseous Oxidized Mercury using HgBr2 at an In-Service AMNet Site, Environmental
453   Science & Technology, 48, 11437-11444, 2014.

454   Miller, M.B. and Gustin, M.S.: Testing and modeling the influence of reclamation and control
455   methods for reducing nonpoint mercury emissions associated with industrial open pit
456   gold mines, Journal of the Air & Waste Management Association, 63, 681-693, 2013.

457   Miller, M.B., Gustin, M.S., and Eckley, C.S.: Measurement and scaling of air-surface mercury
458   exchange from substrates in the vicinity of two Nevada gold mines, Science of the Total
459   Environment, 409, 3879-3886, 2011.

460   Miller, M.B., Gustin, M. S., Dunham-Cheatham, S.S., and Edwards, G.C 2018
461   Evaluation of cation exchange membrane performance under exposure to high Hg^0 and
462        $HgBr_2$ concentrations Atmospheric Measurement Techniques
463   https://doi.org/10.5194/amt-2018-127, 2018
464
465   Obrist, D., Kirk, J., Zhang, L., Sunderland, E., Jiskra, M., Selin, N.: A review of global
466   environmental mercury processes in response to human and natural perturbations:
467   Changes of emissions, climate, and land use, Ambio, 47, 116-140 2018.

468   Pacyna, J., Travnikov, O., De Simone, F., Hedgecock, I., Sundseth, K., Pacyna, E, et al.: Current
469   and future levels of mercury atmospheric pollution on a global scale. Atmospheric
470   Chemistry and Physics; 16, 12495-12511, 2016.

Atmospheric
Measurement
Techniques
Discussions

471   Pierce, A.M., and Gustin, M.S.: Development of a Particulate Mass Measurement System for
472   Quantification of Ambient Reactive Mercury, Environmental Science & Technology 51:
473   436-445, 2017.

474   Pirrone, N., Cinnirella, S., Feng, X., Finkelman, R., Friedli, H., Leaner, J. et al.: Global mercury
475   emissions to the atmosphere from anthropogenic and natural sources, Atmospheric
476   Chemistry and Physics, 10, 5951-5964, 2010.

477
478   Poissant, L., Pilote, M., Xu, X., Zhang, H., and Beauvais, C.: Atmospheric mercury speciation
479   and deposition in the Bay St. Francois wetlands, Journal of Geophysical Research-
        Atmospheres, 109, D11, D11301 **DOI:** 10.1029/2003JD004364
480

481   Rea, A.W., Lindberg, S.E., and Keeler, G.J:. Assessment of Dry Deposition and Foliar Leaching
482   of Mercury and Selected Trace Elements Based on Washed Foliar and Surrogate
483   Surfaces, Environmental Science & Technology, 34, 2418-2425, 2000.

484   Rothenberg, S.E., McKee, L., Gilbreath, A., Yee, D., Connor, M., and Fu, X.: Evidence for
485   short-range transport of atmospheric mercury to a rural, inland site, Atmospheric
486   Environment, 44, 1263-1273, 2010.

487   Sather, M. E., Mukerjee, S., Smith, L., Mathew, J., Jackson, C., Callison, R., et al.: Gaseous
488   oxidized mercury dry deposition measurements in the Four Corners area and Eastern
489   Oklahoma, U.S.A, Atmospheric Pollution Research, 4, 168-180, 2013.

490   Schroeder, W.H., Anlauf, K.G., Barrie, L.A., Lu, J.Y., Steffen, A., Schneeberger, D. R., et al.:
491   Arctic springtime depletion of mercury, Nature, 394, 331, 1998.

492   Skov, H., Brooks, S.B., Goodsite. M.E., Lindberg, S.E., Meyers, T.P., Landis, M. S., et al.:
493   Fluxes of reactive gaseous mercury measured with a newly developed method using
494   relaxed eddy accumulation, Atmospheric Environment, 40, 5452-5463, 2006.

495   Streets, D. G., Horowitz, H. M., Jacob, D. J., Lu, Z., Levin, L., ter Schure, A.F.H., et al. Total
496   Mercury Released to the Environment by Human Activities. Environmental Science &
497   Technology 51, 5969-5977, 2017.

498   UNEP. Minamata Convention on Mercury, 2013.

499   Yannick, A., Théo, Le D., Christopher, W. M., Grant, C. E., and Obrist, D.: New Constraints on
500   Terrestrial Surface–Atmosphere Fluxes of Gaseous Elemental Mercury Using a Global
501   Database, Environmental Science & Technology, 50, 507-524, 2016.

502   Zhang, H. H., Poissant, L., Xu, X., and Pilote, M.: Explorative and innovative dynamic flux bag
503   method development and testing for mercury air–vegetation gas exchange fluxes,
504   Atmospheric Environment, 39, 7481-7493, 2005.

Atmospheric
Measurement
Techniques
Discussions

505   Zhang, L., Lyman, S., Mao, H., Lin, C., Gay, D., Wang, S., et al.: A synthesis of research needs
506   for improving the understanding of atmospheric mercury cycling, Atmospheric
507   Chemistry and Physics,17, 9133-9144, 2017.

508   Zhang, L. M., Wright, L.P., and Blanchard, P.: A review of current knowledge concerning dry
509   deposition of atmospheric mercury, Atmospheric Environment, 43, 5853-5864, 2009.

510   Zhu, W., Lin, C., Wang, X., Sommar, J., Fu, X., and Feng, X.: Global observations and modeling
511   of atmosphere-surface exchange of elemental mercury: a critical review, Atmospheric
512   Chemistry and Physics, 16, 4451-4480, 2016.

513
514
515
516
517
518
519
520
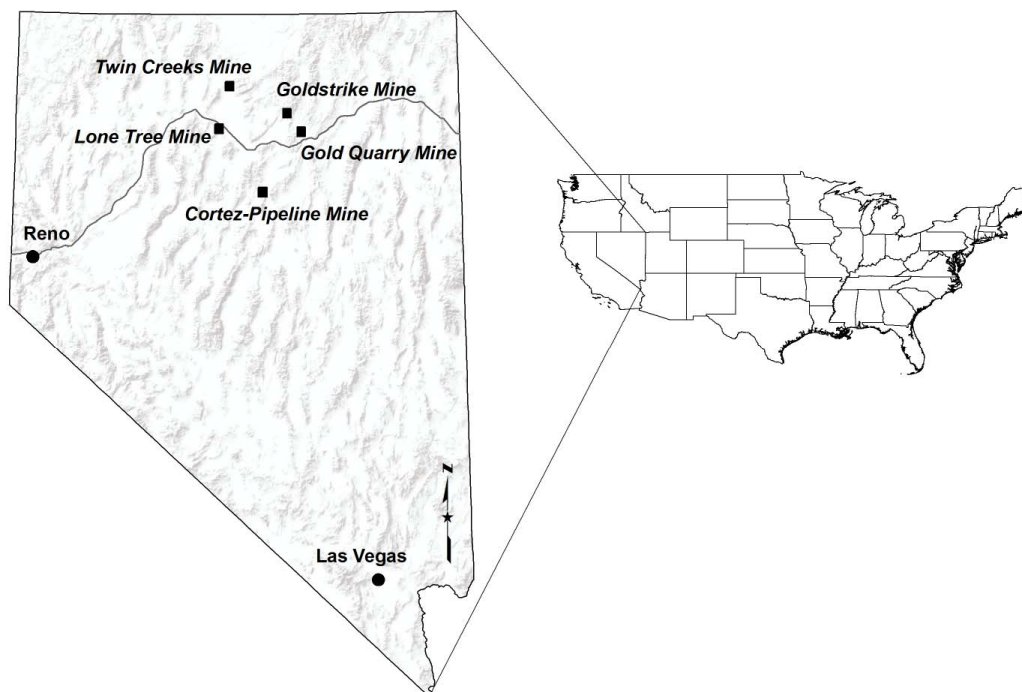
521
522
523   **Figure 1**. Location map of study sites, Nevada, USA (From Miller and Gustin, 2013).

524
525

22

Atmospheric
Measurement
Techniques
Discussions
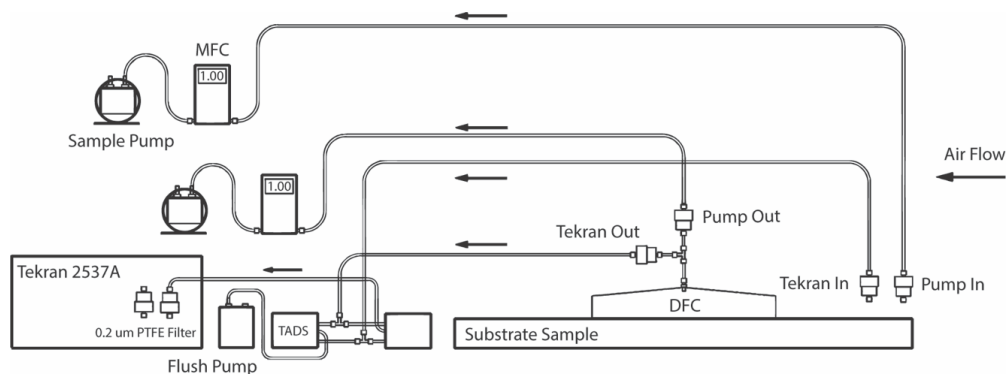
526

527 **Figure 2**. Diagram of one GOM filter-based flux system, deployed in duplicate as Systems A and B..Filter packs
528 indicate the location of the CEM samples.

529

530
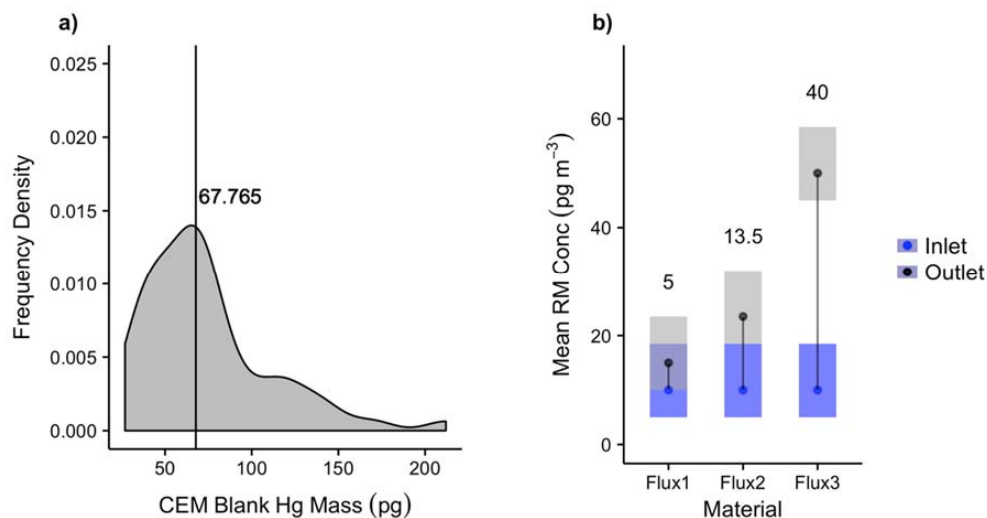
531

532 **Figure 3**. Determination of ΔC_{GOM} detection limit. a) Distribution of Hg mass on unused "blank" CEM filters
533 (median = 68 pg) b) Hypothetical example of statistically detectable GOM flux criteria: shaded boxes represent the
534 maximum uncertainty in concentration, based on 95% confidence interval around the median filter blank (58 – 73
535 pg), Flux1 represents an insufficiently resolvable ΔC_{GOM} in which the 95% confidence intervals around the median
536 blank-corrected C_o and C_i values overlap, Flux2 represents the minimum detectable ΔC_{GOM} (13.5 pg m^{-3}), and Flux3
537 represents an obviously resolvable ΔC_{GOM}.

538
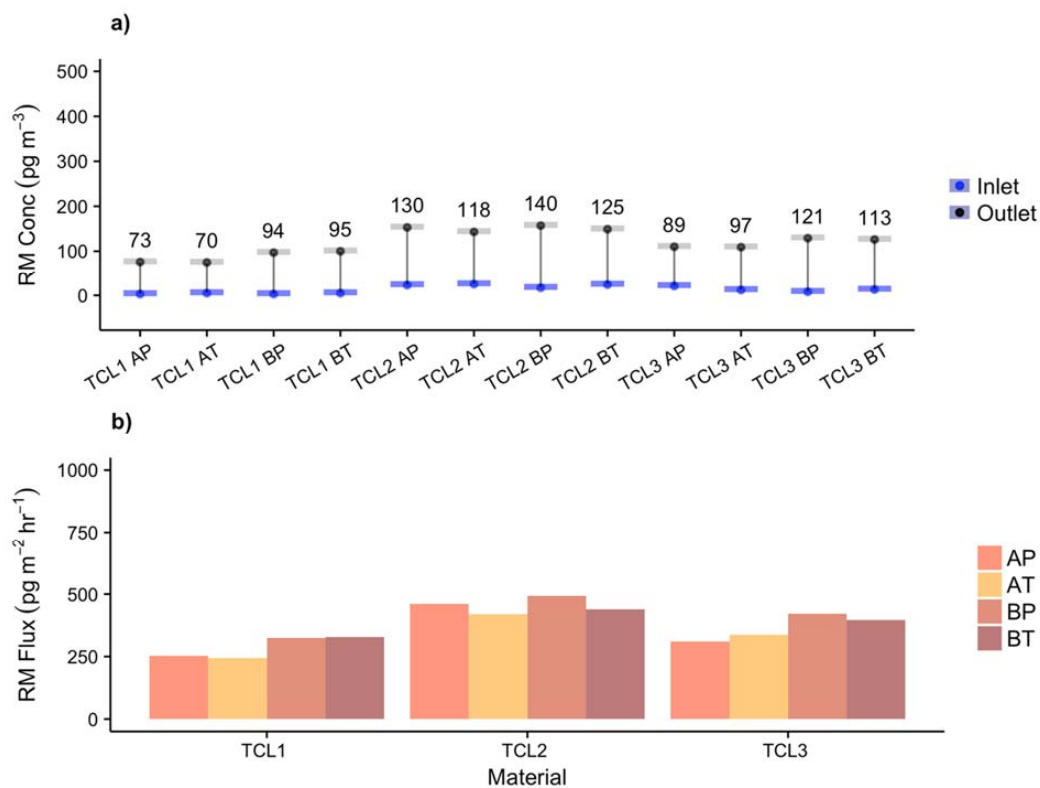
Figure 4. Test 72 h replicate measurements of TCL material. a) ΔC_{GOM} values: grey points indicate chamber concentration (C_o), blue points indicate inlet air concentration (C_i), and the numeric value of ΔC_{GOM} is shown above b) GOM flux from TCL material in three consecutive 72 h measurements, no chamber blank correction. Sample line labels: AP = Pump A, PB = Pump B, AT = Tekran A, BT = Tekran B.

Atmospheric
Measurement
Techniques
Discussions
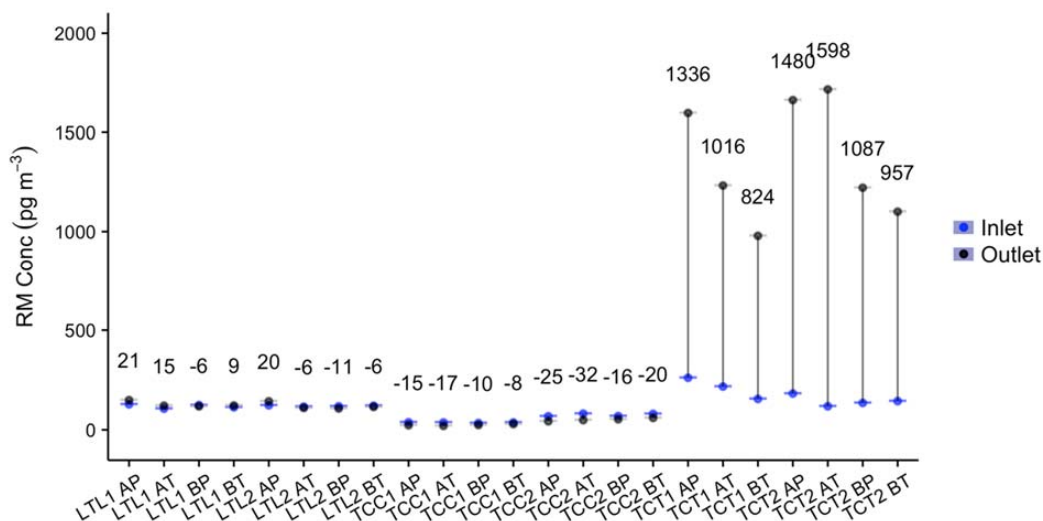

Figure 5. Expanded set of GOM flux measurements for select materials during summer. ΔC_{GOM} was below detection for 5 of 8 LTL measurements, and 2 of 8 TCC measurements, and these values were excluded.
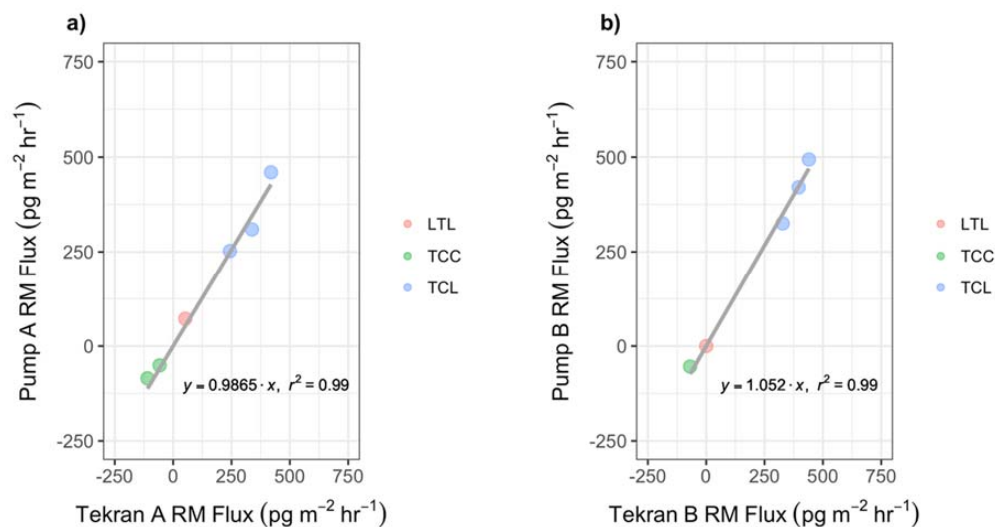
Figure 6. Comparison of GOM fluxes measured by Tekran controlled flow sample lines and external pump flow controlled sample lines, for a) System A and b) System B using TCL, TCC, LTL, and TCT summer measurements. Note TCT data not graphed, as fluxes were an order of magnitude higher and skew the regression r^2 towards 1.

Atmospheric
Measurement
Techniques
Discussions
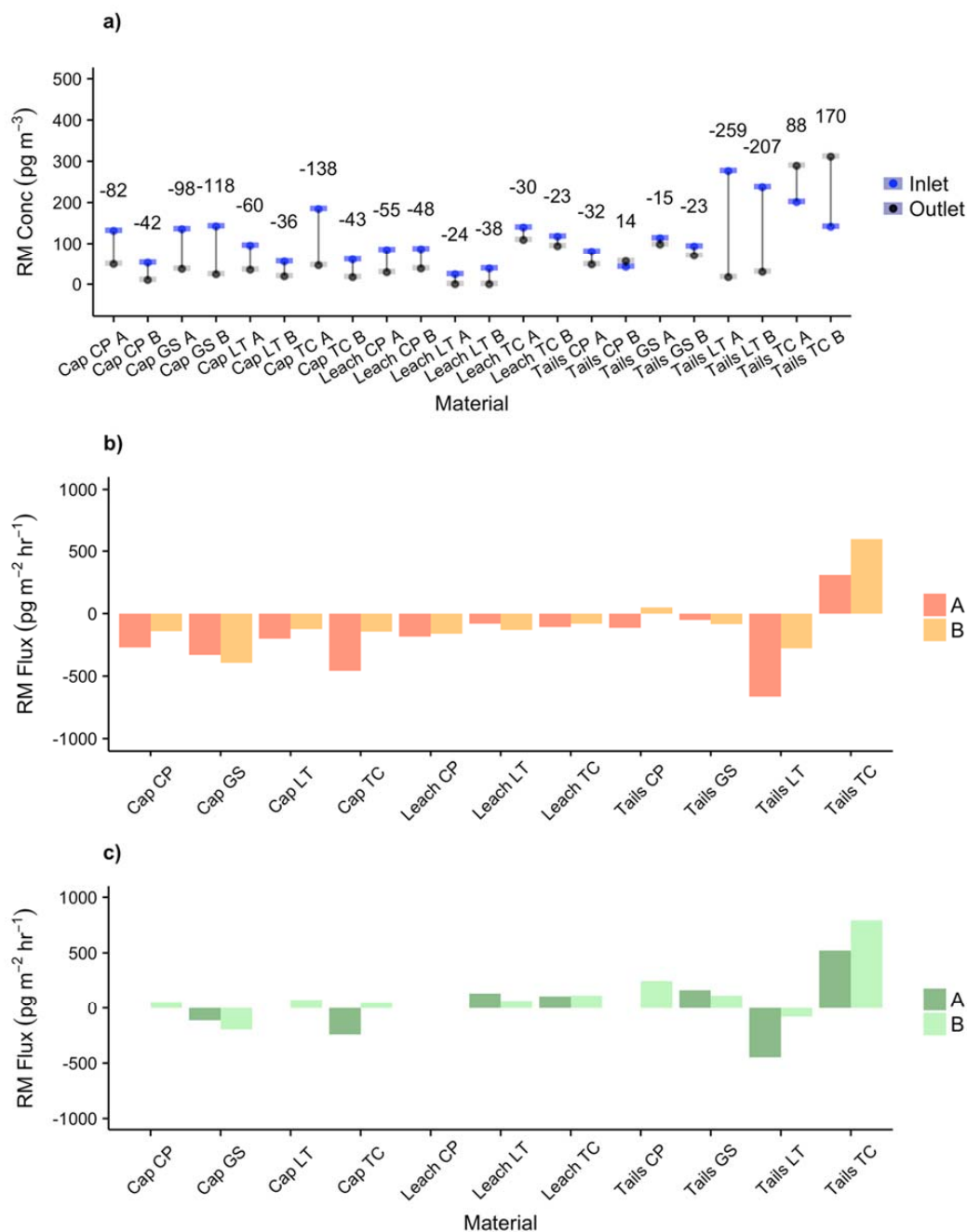
Figure 7. GOM flux measurements for all materials, winter 2016. a) ΔC_{GOM}, above detection limit for all measurements b) GOM flux, no chamber blank correction (shaded orange) c) GOM flux, with chamber blank correction (shaded green).

559
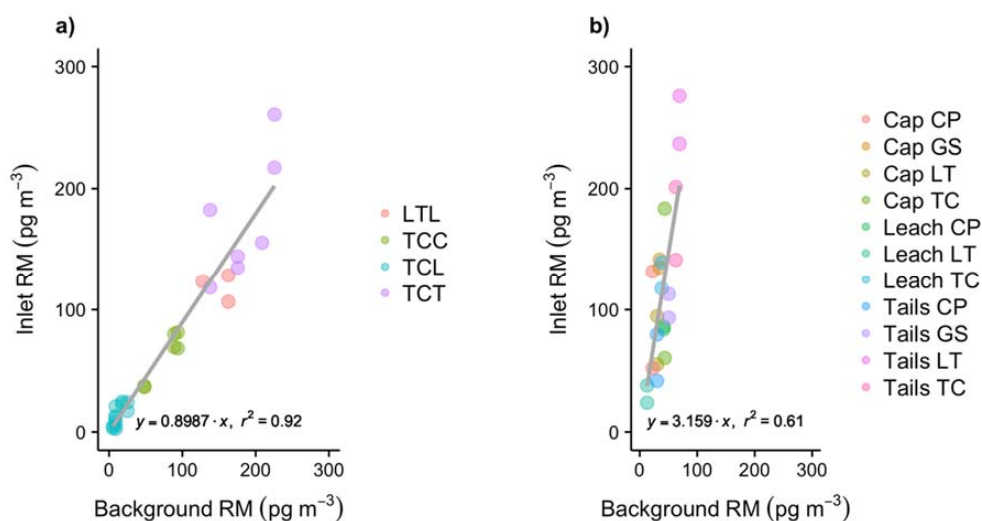
Figure 8. Comparison of ambient background GOM concentrations measured at 2 m height in the greenhouse, vs GOM concentrations measured at the chamber inlet, for a) Summer 2015, and b) Winter 2016. Background vs inlet concentrations were comparable during Summer measurements, but inlet concentrations were much higher relative to background in the winter.

564

565

Table I.

	Material	Sample	Date	Substrate Conc (ng g⁻¹)	GEM Flux (ng m⁻² h⁻¹)	RM Flux (ng m⁻² h⁻¹)	RM Inlet (ng m⁻³)	RM V_d (cm s⁻¹)	Ambient RM (ng m⁻³)	Temp (°C)	RH (%)	Solar (W m⁻²)	Soil Temp (°C)
	Leach	TCL1*	5/16-5/19		134	0.29	0.01	-	0.01				
		TCL2*	5/19-5/22	11900	151	0.45	0.03	-	0.03	na	na	na	na
		TCL3*	5/22-5/25		215	0.37	0.02	-	0.01				
Summer 2015	Cap	TCC1A P	7/21-7/23	230	10	-0.05	0.04	0.04	0.05	22.6	41.6	15.8	23.9
		TCC1A T				-0.06	0.04	0.04					
		TCC1B P			12	na	0.03	na					
		TCC1B T				na	0.04	na					
		TCC2A P	7/29-7/31		4	-0.09	0.07	0.03	0.09	24.8	28.7	15.8	26.4
		TCC2A T				-0.11	0.08	0.04					
		TCC2B P			13	-0.05	0.07	0.02					
		TCC2B T				-0.07	0.08	0.02					
	Leach	LTL1A P	8/12-8/14	590	105	0.07	0.13	-	0.16	23.8	30.2	17.4	26.5
		LTL1A T				0.05	0.11	-					
		LTL1B P			87	na	0.12	na					
		LTL1B T				na	0.11	na					
		LTL2A P	8/14-8/16		100	0.07	0.12	-	0.13	23.4	24.1	17.3	25.6
		LTL2A T				na	0.12	na					
		LTL2B P			99	na	0.12	na					
		LTL2B T				na	0.12	na					
	Tailings	TCT1A P	8/26-8/28	35750	483	4.46	0.26	-	0.22	23.8	31.4	16.6	24.2
		TCT1A T				3.37	0.22	-					
		TCT1B P			370	na	0.15	-					
		TCT1B T				2.76	0.16	-					
		TCT2A P	8/28-8/31		702	5.02	0.18	-	0.16	22.0	33.3	13.9	22.1
		TCT2A T				5.43	0.12	-					
		TCT2B P			457	3.02	0.13	-					
		TCT2B T				2.57	0.14	-					
Winter 2016	Cap	TCCA	1/6/16	230	1	-0.24	0.18	0.07	0.04	15.0	37.6	2.7	14.5
		TCCB			1	0.05	0.06	-					
		LTCA	1/7/16	150	0	0.00	0.09	-	0.03	14.5	38.6	9.7	11.8
		LTCB			-1	0.07	0.06	-					
		CPCA	1/20/16	120	-1	0.00	0.13	-	0.02	14.5	31.7	12.9	15.6
		CPCB			na	0.06	0.05	-					
		GSCA	1/21/16	200	-1	-0.12	0.13	0.02	0.03	14.6	26.6	11.0	15.8
		GSCB			-1	-0.20	0.14	0.04					
	Leach	TCLA	1/26/16	11900	29	0.11	0.14	-	0.04	13.4	35.3	9.3	15.2
		TCLB			30	0.11	0.12	-					
		CPLA	1/29/16	310	-18	0.00	0.08	-	0.04	13.9	34.9	16.5	15.3
		CPLB			-12	0.00	0.09	-					
		LTLA	2/2/16	590	-4	0.13	0.02	-	0.01	11.7	25.5	14.6	14.2
		LTLB			-3	0.07	0.04	-					
	Tailings	CPTA	2/9/16	21150	4	0.00	0.08	-	0.03	14.1	37.5	18.9	15.7
		CPTB			5	0.25	0.04	-					
		GSTA	2/10/16	6960	16	0.16	0.11	-	0.05	14.4	39.3	11.6	13.8
		GSTB			-1	0.11	0.09	-					
		LTTA	3/20/16	11020	2	-0.45	0.28	0.05	0.07	19.8	23.1	31.0	22.3
		LTTB			2	-0.08	0.24	0.01					
		TCTA	3/22/16	35750	51	0.52	0.20	-	0.06	17.0	26.6	37.4	19.3
		TCTB			71	0.79	0.14	-					

Table I. Summary of GEM and GOM flux and ambient parameters for all measurements. Fluxes are chamber blank-corrected where applicable, and V_d values are based on corrected fluxes (- indicates no deposition, *na* indicates non-detectable flux).